

True nature of active layers in organic solar cells fabricated by sequential casting of donor and acceptor layers

Jong Hyuk Yim^{**}, Sung-yoon Joe^{**}, Duc Cuong Nguyen, Shin Young Ryu, Na Young Ha, Y. H. Ahn, Ji-yong Park, and Soonil Lee^{*}

Department of Physics and Division of Energy Systems Research, Ajou University, Suwon 16499, Korea

Received 1 December 2016, revised 16 December 2016, accepted 16 December 2016

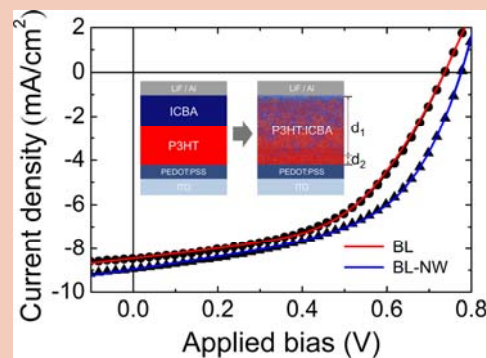
Published online 23 December 2016

Keywords organic solar cells, bulk heterojunctions, P3HT, nanowires, ICBA, device simulation

* Corresponding author: e-mail soonil@ajou.ac.kr, Phone: +82 31 219 2582, Fax: +82 31 219 1748

** These authors contributed equally to this work.

The operation characteristics of nominal bilayer (BL) organic solar cells (OSCs), the active layers (ALs) of which consisted of sequentially casted bottom P3HT donor and top ICBA acceptor layers, resembled those of OSCs with bulk heterojunction (BHJ) ALs. Optical analysis and device simulations showed that such resemblance can be attributed to a similarity in the micromorphology of ALs; as-deposited BL-type ALs transformed spontaneously into BHJ-type ALs. The inclusion of P3HT nanowires (NWs) in the donor layers resulted in different AL micromorphology and consequently a larger power conversion efficiency. Separate assessment of the exciton generation and charge–carrier transport and/or extraction showed that the contribution of P3HT NWs was more prominent in optical effects.



Transformation of sequentially casted P3HT and ICBA layers into a bulk heterojunction layer accounts for good agreement between measured and simulated J – V curves.

© 2017 WILEY-VCH Verlag GmbH & Co. KGaA, Weinheim

1 Introduction Elucidation of the role of P3HT donor nanowires (NWs) in enhancing performance of organic solar cells (OSCs) that consists of a judiciously selected donor–acceptor pair has been a challenging research topic [1–5]. Separate appraisal of optical and electrical effects attributable to P3HT NWs is of particular interest. Another challenge lies in identifying the true nature of active layers (ALs) of bilayer (BL) OSCs, which nominally consisted of top acceptor (i.e. ICBA) and bottom donor (i.e. P3HT) layers. There were only a few previous reports of pseudo-bilayer OSCs, AL morphology of which were very similar to that of bulk heterojunction (BHJ) OSCs in spite of separate spin-coating of acceptor and donor layers in sequence

[6]. Diffusion of ICBA molecules into a P3HT layer was proposed as a plausible model for pseudo-bilayer OSCs [7–10]. Adding P3HT NWs in donor layers can bring a new aspect in BL OSCs because a porous P3HT-NW network becomes a supporting structure for bottom layers. Because preformed P3HT NWs remain intact even after exposure to a solvent for subsequent ICBA casting, ICBA diffusion and distribution in NW-containing donor layers can be different from those in pristine P3HT layers [2]. Consequently, discrepancy in optical and electrical effects can result from the inclusion of P3HT NWs in bottom donor layers.

In this work, we studied the eventual microstructure of sequentially coated donor–acceptor bilayer ALs by com-

bining optical spectrum analysis based on an effective medium theory with device performance simulations. In our solar cell simulations, realistic exciton generation profiles were estimated from the effective optical constants of ALs. Additionally, a model of fictitious semiconductor with hole and electron traps was assumed for simulations of current density (J) variations with respect to voltage (V). With good agreement between experimental and simulated J - V curves, we were able to assess optical and electrical contributions of P3HT NWs to performance improvements of OSCs, separately.

2 Experiment and simulation OSCs were made by sequentially spin-coating P3HT donor and ICBA acceptor layers on top of PEDOT:PSS layers formed on ITO-coated glasses ($12 \Omega \text{ sq}^{-1}$, GEOMATEC). OSC fabrication was completed with the deposition of LiF/Al cathodes by evaporation. DCB solutions of pristine P3HT (20 mg/ml) were used as-prepared or after mixing with another solution of pre-formed P3HT NWs in DCM (24 mg/ml) to cast donor layers. A name convention of BL and BL-NW were used to identify OSCs according to their donor layer types. The NW-containing donor solution was stirred over 24 h at room temperature before spin-coating. Acceptor solutions were prepared by dissolving 10 mg of ICBA in DCM at 60 °C under continuous stirring over 24 hours. Donor layers were spin-coated at 800 rpm for 30 s and heat-treated at 140 °C on a hot plate for 10 min. However, acceptor layers were spin-coated at 3000 rpm for 10 s and then baked at 150 °C for 30 min.

The cell size, defined by the overlap of cathode and anode electrodes, was 0.24 cm². OSC operations were measured under AM 1.5G illumination at 1 sun by using a solar simulator (PEC-L01, Peccell) that was calibrated to 100 mW/cm² with a reference Si cell (PEC-S101, Peccell). Transmittance, reflectance, and absorbance spectra were measured by using a spectrophotometer (Cary 5000, Varian).

Operation of the two OSCs were simulated using a device simulator SCAPS developed by Burgelman's group at the University of Gent (ver. 3.3.03), which is basically a drift-diffusion equation solver [11]. Details of SCAPS simulations are specified in Supporting Information and Tables therein.

3 Results and discussion Experimental J - V curves in Fig. 1(a) show that performance of the device BL-NW is superior to that of the device BL. Specifically, performance parameters of the device BL were open-circuit voltage (V_{OC}) of 0.740 V, short-circuit current (J_{SC}) of 8.40 mA/cm², fill factor (FF) of 51.3%, and PCE of 3.19%. On the other hand, improved J_{SC} , V_{OC} , and FF of the device BL-NW were 8.94 mA/cm², 0.777 V, and 52.3%, respectively. Correspondingly, PCE was improved by 13.8%, attaining a higher PCE of 3.63%. In addition to overall performance improvements in response to the inclusion of P3HT-NWs, we noted that performance of the BL OSCs,

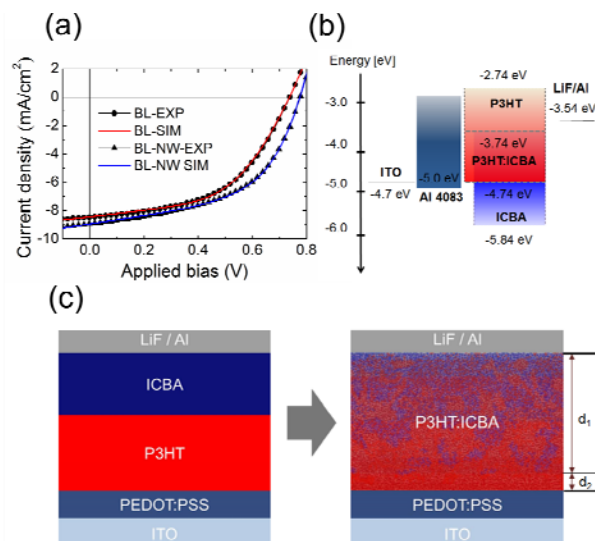


Figure 1 (a) Measured (symbols) and simulated (solid lines) J - V curves for BL and BL-NW OSCs, respectively. (b) Energy level diagram of the materials used for OSC fabrication. Grey dash lines corresponding to P3HT's LUMO and ICBA's HOMO were considered as electron- and hole-traps in a fictitious organic semiconductor, LUMO and HOMO of which were assumed to coincide with ICBA's LUMO and P3HT's HOMO, respectively. (c) Schematic representation of active-layer morphology change; the original active layer of sequentially-casted separate layers of P3HT and ICBA transformed into a structure that consisted of a BHJ-like layer of thickness d_1 and a remnant pure donor layer of thickness d_2 . The simulated J - V curves in (a) correspond to the common d_1 of 168 nm for a BHJ-like layer, and d_2 of 19 nm and 32 nm for an unblended P3HT layer for the BL and BL-NW device, respectively.

with or without P3HT-NW inclusion, was not very much different from those of corresponding BHJ OSCs. Small discrepancy in operation characteristics of nominal BL and BHJ OSCs led us to consider the possibility that ALs of the two types of OSCs were in fact similar regardless of P3HT-NW inclusion. To manifest the true nature of ALs in the two nominal BL-type OSCs, we performed J - V curve simulations based on the energy level diagram in Fig. 1(b). Surprisingly, SCAPS simulations based on a BL-type ALs were unable to reproduce measured J - V curves of both devices, regardless of P3HT-NW inclusion. Wide-range adjustments of structure and material parameters were of no use in producing reasonably good agreement between measured and simulated J - V curves. On the contrary, when we used the transformed AL morphology shown in Fig. 1(c), SCAPS simulations produced J - V curves that agreed very well with experimental ones as seen in Fig. 1(a). Successful simulation of inorganic solar cells (ISCs) with the device simulator SCAPS was done previously. ISC simulations are straightforward because device structures can be precisely specified, and physical property parameters of typical inorganic semiconductors are readily available from literature. Accordingly, light harvesting and exciton generation can be accounted for quantitatively, and

charge carrier transport and extraction can be taken into account accurately.

However, it is not the case for BHJ OSC simulations. Specification of both micromorphology and intrinsic material properties of BHJ ALs for SCAPS simulations were not straightforward. To circumvent these difficulties, we simplified spontaneously formed AL structures as two sub-layers seen in Fig. 2(c). Moreover, we represented optical and electronic properties of an upper BHJ-like sublayer by using effective optical constants and energy levels of a fictitious organic semiconductor, respectively. It is worth emphasizing that a single-layer model was unable to fit experimental reflectance spectra and J - V curves simultaneously. Effective optical constants were determined by fitting transmittance spectra of nominal bilayers of ICBA and P3HT (with or without NW inclusion), which were spin-coated on glass substrates following the same exact recipe for ALs of the device BL and BL-NW. The use of effective medium approximation (EMA) with optical constants of AL constituents, such as ICBA, P3HT, and P3HT NW, to model BHJ-like upper layers were successful in producing good fitting curves to experimental spectra as shown in Fig. 2(a) and (b). The fitted curves correspond to the same d_1 of 168 nm for a BHJ-like layer, and d_2 of 19 nm and 32 nm for an unblended P3HT layer for the device BL and BL-NW, respectively. EMA modelling results were used to calculate position- and wavelength-dependent exciton generation rates in respective ALs, the integration of which resulted in variations of exciton generation rates with respect to wavelength and thickness as seen in Fig. 2(c). We note that exciton generation was more efficient in the case of BL-NW's AL, in particular, in a long-wavelength range, and that exciton generation was more evenly distributed in the middle of a BHJ-like layer as shown in the inset of Fig. 2(c). Both of these characteristics were proven advantageous for higher PCE. The exciton generation rates in Fig. 2(c) were imported to the device simulator SCAPS and used for J - V curve simulations.

In J - V simulations, we modeled the BHJ-like sublayer as a fictitious semiconductor having the lowest unoccupied (LUMO) and highest occupied (HOMO) molecular orbital which coincide with ICBA's LUMO and P3HT's HOMO, respectively. We argue that this model is appropriate to take into account transport of electrons and holes in real OSCs because electron and hole transport in BHJ ALs occur separately along a percolating path of P3HT or that of ICBA. Additionally, we treated P3HT's LUMO and ICBA's HOMO as electron and hole traps, respectively. SCAPS simulations based on our fictitious semiconductor model, sublayer thicknesses estimated from the fitting of transmittance spectra, and the imported exciton generation rate profiles were able to reproduce J - V curves that showed good agreement with experimental data. All parameter values we used for J - V simulations are listed in Table S1 in Supporting Information.

Successful J - V curve simulations for both device types, BL and BL-NW, allowed us to investigate the effects that P3HT NWs contributed further. Initially, the inclusion of P3HT NWs, hole mobility of which was reported to be higher than that of pristine P3HT, was expected to improve FF and accordingly PCE. However, we found that increase of hole mobility brought degradation to OSC performance seen in Fig. 3(a). Quantitatively, hole mobility 10 times larger compared to the value corresponding to the fitting curve in Fig. 1(a) resulted in 16.6% reduction of FF (from 52.5% to 43.8%) and 3.45% decrease of J_{SC} (from 8.95 mA/cm² to 8.64 mA/cm²), which combined to make PCE reduced by 19.0% (from 3.64% to 2.95%); see the inset of Fig. 3(a). Phenomenologically, smaller shunt resistance in response to larger hole mobility was responsible for prominent FF degradation. Small photoshuttle resistance is typically linked to excessive recombination loss. In short, unbalanced hole mobility increase may cause imbalance in hole and electron extraction and can not necessarily ensure OSC performance improvement.

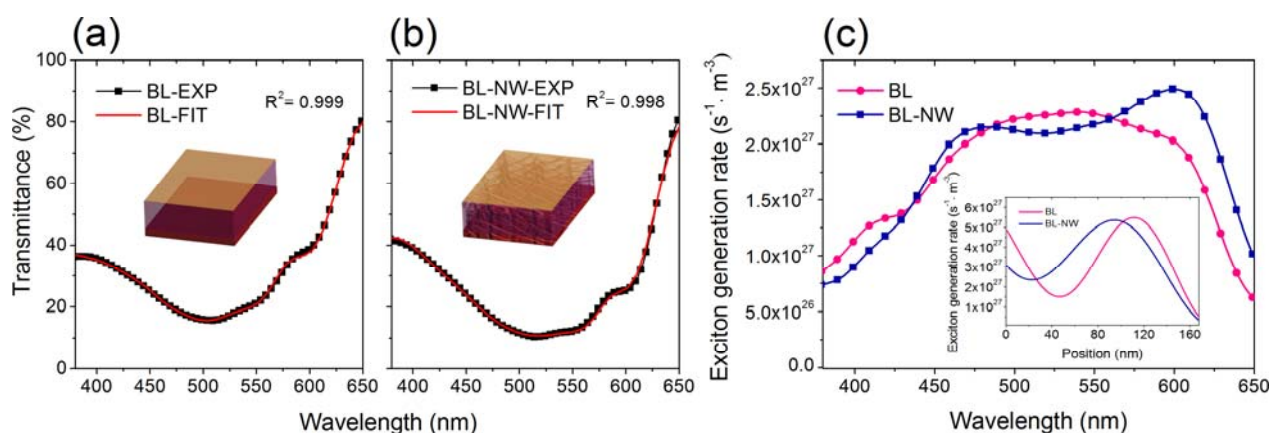


Figure 2 Optical transmittance spectra for nominal bilayers of ICBA and P3HT, sequentially casted on glass substrates following the same exact recipe for active layers of the device (a) BL and (b) BL-NW. Symbols are experimental data, and solid lines are fitting curves based on effective-medium-approximation models. (c) Exciton generation rates of the BL and BL-NW devices with respect to wavelength. Inset shows position-dependent exciton generation rates in active layers from $x = 0$ (bottom) to 168 (top) nm.

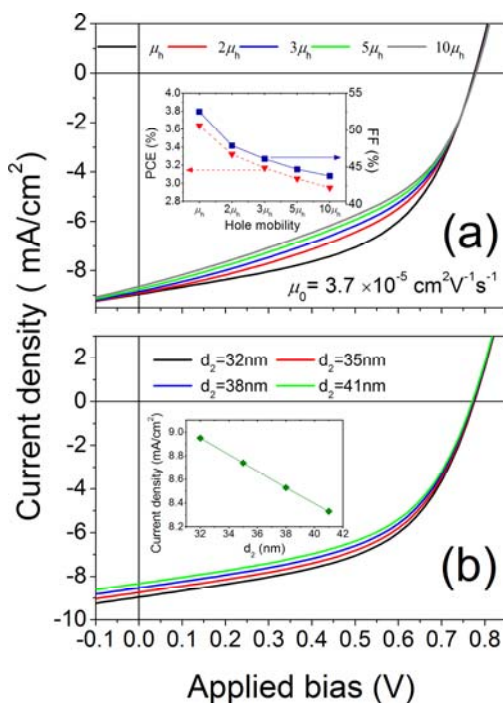


Figure 3 Variations of simulated J - V curve for BL-NW devices with respect to (a) hole mobility μ_h and (b) bottom layer thickness d_2 . Insets in (a) and (b) show μ_h dependence of PCE and FF, and d_2 dependence of current densities, respectively. Electron mobility μ_e was kept fixed at $5 \times 10^{-5} \text{ cm}^2 \text{ V}^{-1} \text{ s}^{-1}$ [12]. Solar cell performance parameters corresponding to the J - V curves in Fig. 3(a) and (b) are listed in Tables in S2 and S3, respectively.

Different behavior appeared in response to d_2 increase as seen in Fig. 3(b). In this case, V_{OC} decrease appeared in addition to similar FF and J_{SC} reduction. Quantitatively, 9 nm increase of d_2 (from 32 nm to 41 nm) induced 0.80% reduction of V_{OC} (from 0.776 V to 0.770 V), and the decrease of FF and J_{SC} by 2.48 (from 52.5% to 51.2%) and 6.93% (from 8.95 mA/cm² to 8.33 mA/cm²), respectively. All changes in V_{OC} , FF, and J_{SC} combined to result in PCE reduction of 9.62% (from 3.64% to 3.29%); see the inset of Fig. 3(b). Overall degradation of OSC performance with respect to d_2 increase was not surprising at all because most of carriers generated in the bottom P3HT sublayers were bound to be lost due to recombination. In this respect, spontaneous formation of a BHJ-like sublayer in nominal bilayer OSCs was essential for good performance.

4 Conclusion The combination of non-destructive optical analysis and J - V curve simulations provided us with strong evidence for spontaneous transformation of sequentially spin-coated P3HT and ICBA layers into a two sublayer AL structure that consisted of an upper BHJ-like sublayer and a lower pristine P3HT layer. Because the upper BHJ-like sublayer was mostly responsible for solar photon harvesting to generate excitons and charge carrier

transport, it was not surprising to find that performance of nominal BL OSCs were very similar to that of conventional BHJ OSCs. Spontaneous formation of a BHJ-like sublayer from sequentially casted donor and acceptor layers can be taken advantage of for more elaborate control of active layer structures. For example, alternating casting of donor and acceptor materials multiple times can be a useful recipe for further optimization of micromorphology of active layers. In particular, utilization of preformed P3HT NWs which are advantageous for more efficient solar photon absorption and remain intact after exposure to many common solvents will allow for more diverse approaches in developing highly optimized active layers and/or OSC architectures.

Supporting Information Additional supporting information may be found in the online version of this article at the publisher's website. There, details of SCAPS simulation models, simulation parameter values, solar cell parameters corresponding to simulation results in Fig. 3, AFM images showing surface morphology of donor and completed active layers, and additional J - V simulation results corresponding to thicker d_2 are included.

Acknowledgements This research was supported by the National Research Foundation of Korea (NRF) Grant (No. NRF-2014R1A2A2A01005632) which is funded by the Korea government (MEST).

References

- [1] J.-H. Kim, J. H. Park, J. H. Lee, J. S. Kim, M. Sim, C. Shim, and K. Cho, *J. Mater. Chem.* **20**, 7398 (2010).
- [2] S. Y. Joe, J. H. Yim, S. Y. Ryu, N. Y. Ha, Y. H. Ahn, J. Y. Park, and S. Lee, *Chem. Phys. Chem.* **16**, 1217 (2015).
- [3] J. H. Kim, M. Kim, H. Jinnai, T. J. Shin, H. Kim, J. H. Park, S. B. Jo, and K. Cho, *ACS Appl. Mater. Interfaces* **6**, 5640 (2014).
- [4] M. He, L. Zhao, J. Wang, W. Han, Y. Yang, F. Qiu, and Z. Lin, *ACS Nano* **4**, 3241 (2010).
- [5] M. He, W. Han, J. Ge, Y. Yang, F. Qiu, and Z. Lin, *Energy Environ. Sci.* **4**, 2894 (2011).
- [6] L. N. S. A. Thummala, C. H. Yong, K. Ananthanarayanan, and J. Luther, *Org. Electron. Phys. Mater. Appl.* **13**, 2008 (2012).
- [7] A. L. Ayzner, C. J. Tassone, S. H. Tolbert, and B. J. Schwartz, *J. Phys. Chem. C* **113**, 20050 (2009).
- [8] K. H. Lee, P. E. Schwenn, A. R. G. Smith, H. Cavaye, P. E. Shaw, M. James, K. B. Krueger, I. R. Gentle, P. Meredith, and P. L. Burn, *Adv. Mater.* **23**, 766 (2011).
- [9] D. Chen, F. Liu, C. Wang, A. Nakahara, and T. P. Russell, *Nano Lett.* **11**, 2071 (2011).
- [10] M. K. Wong and K. Y. Wong, *Synth. Met.* **170**, 1 (2013).
- [11] M. Burgelman, P. Nollet, and S. Degraeve, *Thin Solid Films* **361–362**, 527 (2000).
- [12] D. Gao, B. Djukic, W. Shi, C. R. Bridges, L. M. Kozycz, and D. S. Seferos, *ACS Appl. Mater. Interfaces* **5**, 8038 (2013).